8-Hydroxyquinoline Schiff-base Compounds as Antioxidants and Modulators of Copper-Mediated Aβ Peptide Aggregation

Luiza M. F. Gomes [a,b]; Rafael P. Vieira[a,b]; Michael R. Jones[b]; Michael C. P. Wang[b]; Christine Dyrager[b] Elaine M. Souza-Fagundes[c]; Jeferson G. Da Silva[a]; Tim Storr[b]; Heloisa Beraldo[a]**

[a]*Departamento de Química, Universidade Federal de Minas Gerais, 31270-901, Belo Horizonte, MG, Brazil*

[b]*Department of Chemistry, Simon Fraser University, V5A-1S6, Burnaby, BC, Canada*

[c]*Instituto de Ciências Biológicas, Universidade Federal de Minas Gerais, 31270-901, Belo Horizonte, MG, Brazil*

*tim_storr@sfu.ca; hberaldo@ufmg.br

Abstract

One of the hallmarks of Alzheimer's disease (AD) in the brain are amyloid-β (Aβ) plaques, and metal ions such as copper(II) and zinc(II) have been shown to play a role in the aggregation and toxicity of the Aβ peptide, the major constituent of these extracellular aggregates. Metal binding agents can promote the disaggregation of Aβ plaques, and have shown promise as AD therapeutics. Herein, we describe the syntheses and characterization of an acetohydrazone (8-H_2QH), a thiosemicarbazone (8-H_2QT), and a semicarbazone (8-H_2QS) derived from 8-hydroxyquinoline. The three compounds are shown to be neutral at pH 7.4, and are potent antioxidants as measured by a Trolox Equivalent Antioxidant Capacity (TEAC) assay. The ligands form complexes with Cu^{II}, 8-H_2QT in a 1:1 metal:ligand ratio, and 8-H_2QH and 8-H_2QS in a 1:2 metal:ligand ratio. A preliminary aggregation inhibition assay using the $A\beta_{1\text{-}40}$ peptide showed that 8-H_2QS and 8-H_2QH inhibit peptide aggregation in the presence of Cu^{II}. Native gel electrophoresis/Western blot and TEM images were obtained to give a more detailed picture of the extent and pathways of Aβ aggregation using the more neurotoxic $A\beta_{1\text{–}42}$ in the presence and absence of Cu^{II}, 8-H_2QH, 8-H_2QS and the drug candidate PBT2. An increase in the formation of oligomeric species is evident in the presence of Cu^{II}.

Corresponding author. Phone: Tim Storr +17787828657;
Heloisa Beraldo +55 3134095740

However, in the presence of ligands and Cu^{II}, the results match those for the peptide alone, suggesting that the ligands function by sequestering Cu^{II} and limiting oligomer formation in this assay.

Keywords: 8-hydroxyquinoline; Copper (II) complex; Alzheimer's disease.
Note: Luiza M. F. Gomes and Rafael P. Vieira contributed equally to this work.

Corresponding author. Phone: Tim Storr +17787828657;
Heloisa Beraldo +55 3134095740

1. Introduction

Dementias are progressive pathophysiological disorders characterized by neuronal cell loss and severe cognitive impairment.[1-3] The higher prevalence of these neurodegenerative processes in the elderly, and the increased life expectancy in many countries, represents a significant burden on healthcare systems around the globe. There are over 35 million people worldwide displaying dementia symptoms and this number is expected to double by 2030 (65.7 million) and more than triple by 2050 (115.4 million).[2, 4-5] Alzheimer's Disease (AD) is the most common type of dementia and is characterized by oxidative stress, misfolded proteins, neuronal cell loss, and eventually death.[2, 6-7] The mechanism underlying the causes and progression of AD is subject to enormous research efforts, and the search for new and effective therapies is justified by the lack of effective treatment options.[8-9]

Diagnosis of AD, as opposed to other forms of dementia, requires *post-mortem* examination of the brain to determine the severity of neuropathological hallmarks of the disease; amyloid-beta (Aβ) plaques and neurofibrillary tangles. Neurofibrillary tangles are intracellular fibrillar aggregates of oxidatively-modified and hyperphosphorylated microtubule-associated protein tau.[10] Aβ-plaques are extracellular deposits of fibrils and amorphous aggregates of the Aβ peptide (*vide infra*). The amyloid hypothesis has long been the dominant theory to explain the cause of AD, postulating that Aβ plaque depositions, or partially aggregated soluble Aβ, trigger a neurotoxic cascade causing AD pathology.[11-13] Soluble forms of Aβ better correlate with memory impairment and AD progression in comparison to Aβ plaques,[14] however, nearly all aggregated forms exhibit toxicity. Metal ions, such as Cu^{II}, Zn^{II} and Fe^{III} exhibit a relatively high binding affinity with the Aβ peptide,[15-18] and this process can modulate aggregation,[19-21] induce

the formation toxic oligomers and reactive oxygen species (ROS) leading to oxidative stress.[22-23] Aβ plaques are the most prominent pathological feature of AD, however soluble oligomeric forms of the peptide (approximately 1% of total Aβ in brain) have been found to show a better correlation with disease progression.[14, 24-25] When Zn^{II} binds to Aβ there is an increase in the formation of non-fibrillar aggregates[22, 26] without causing an oxidative cascade, whereas the Cu^{II} - Aβ interaction generates non-fibrillar aggregates (oligomer stabilization)[22, 27-29] and oxidative damage likely via ROS generation.[30] Cellular toxicity studies in neuroblastoma cell lines have shown that Zn^{II} reduces $A\beta_{1-42}$ toxicity, while Cu^{II} significantly increases $A\beta_{1-42}$ neurotoxicity.[22] For these reasons, despite the fact that both Cu^{II} and Zn^{II} precipitate Aβ, it has been postulated that the Zn^{II} - Aβ interaction exhibits an overall protective effect in the brain.[26, 30] We have thus chosen to focus on modulating the Cu^{II} - Aβ interaction in this work.

The development of metal-protein attenuating compounds (MPAC) is a promising therapeutic approach for AD treatment. Targeting the metal-Aβ interaction in the extracellular environment could normalize the distribution of both metal ions and Aβ peptide in brain tissue and cerebrospinal fluid.[24, 31-34] Clioquinol (5-chloro-7-iodo-8-hydroxyquinoline, HCQ, Fig. 1) is a small, lipophilic and bioavailable metal chelator, with high selectivity for Zn^{II} and Cu^{II}, that has been reported to cross the BBB efficiently in the Tg2576 mouse model.[4, 35] HCQ is the archetypical MPAC, and has shown promise as an AD therapeutic in both animal models and preliminary clinical trials.[2, 35-36] A second generation 8-hydroxyquinoline derivative, PBT2 (Fig. 1), demonstrated therapeutic potential in AD murine models,[37-38] and Phase II clinical studies.[39-40] This compound has been shown to reduce Aβ aggregation, limit Aβ oligomer toxicity, and redistribute metal ions (Cu^{II} and Zn^{II}) into neurons.[2, 34] A number

of other chemical scaffolds have shown promise as prototype MPAC's for AD therapy.[9, 29, 41-48] In this work we have studied Schiff-bases derived from 8-hydroxy-2-quinolincarboxaldehyde as new MPAC for AD therapy. Hydrazones, semicarbazones and thiosemicarbazones are Schiff-bases that have shown broad pharmacological application and their mechanisms of action frequently involve metal-chelating properties *in vivo*.[49] Triapine (3-aminopyridine-2-carboxaldehyde thiosemicarbazone) is a promising Schiff base that is currently being investigated in several Phase II clinical trials for cancer therapy; whose pharmacological activity involves iron chelation.[50-54] Furthermore, it has shown effectiveness in preventing or reducing ROS accumulation and the concomitant oxidative damage in both AD-derived and age-matched olfactory neuroepithelial cells.[55]

Insert Fig. 1

Herein, we have studied the Schiff base compounds 2-[(8-Hydroxyquinolinyl)methylene]acetohydrazide (8-H_2QH), 2-[(8-Hydroxyquinolinyl)methylene]hydrazinecarboxamide (8-H_2QS), and 2-[(8-Hydroxyquinolinyl)methylene]hydrazinecarbothioamide[56] (8-H_2QT) where H_2L stands for the neutral compound (Fig. 1). These compounds can bind transition metals in bidentate, tridentate or tetradentate coordination modes.[56-58] The characterization of the Cu^{II} chelation and Aβ interaction properties of 8-H_2QH and 8-H_2QS are reported along with the evaluation of their ability to modulate Aβ aggregation.

2. Experimental

All common chemicals were purchased from Aldrich and used without further purification. The syntheses of the ligands 2-[(8-

Hydroxyquinolinyl)methylene]acetohydrazide (8-H_2QH), 2-[(8-Hydroxyquinolinyl)methylene]hydrazinecarboxamide (8-H_2QS), 2-[(8-Hydroxyquinolinyl)methylene]hydrazinecarbothioamide (8-H_2QT), and their Cu^{II} complexes were performed using previously described methodologies.[56-57] PBT2 was synthesized according to a reported method.[59] The ligand 8-H_2QS was previously obtained in its hydrochloride form,[58] herein the neutral form was prepared. The Cu^{II} complex of 8-H_2QT (Cu(8-QT)) was synthesized as reported.[57] The $A\beta_{1–40}$ and $A\beta_{1–42}$ peptides were purchased from 21st Century Biochemicals (Marlborough, MA, USA). The 10-20% Tris-tricine mini gels were purchased from BioRad and membranes from PALL – Life Sciences. ^{1}H and ^{13}C NMR spectra were recorded on a Bruker AV-600 instrument. Mass spectra (positive ion) were obtained on an Agilent 6210 time-of-flight electrospray ionization mass spectrometer. Electronic spectra were obtained on a Cary 5000 spectrophotometer. Magnetic susceptibilities were measured on a Johnson Matthey MSB/AUTO balance. Elemental analyses were performed on a Perkin Elmer CHN 2400 analyzer. A YSI model 31 conductivity bridge was employed for molar conductivity measurements. Infrared spectra were recorded on a Perkin Elmer FT-IR Spectrum GX spectrometer using KBr plates (4000 – 400 cm^{-1}) and CsI/nujol (600 – 200 cm^{-1}).

2.1. Synthesis of 2-[(8-Hydroxyquinolinyl)methylene]acetohydrazide (8-H_2QH)

8-hydroxy-2-quinolincarboxaldehyde (0.173 g, 1 mmol) was suspended in ethanol (10 mL) and treated with an excess of acethydrazide (0.081 g, 1.1 mmol). The reaction mixture was subsequently refluxed for 4 h. The light yellow precipitate that formed was washed with water, ethanol and diethyl ether, air-dried and isolated in good yield (89%) and purity. Mp: 224.1 – 225.1 °C. Elemental Found (calcd) for $C_{12}H_{11}N_3O_2$: C, 62.83

(62.87); H 4.95 (4.84); N 18.26 (18.33). ^{1}H NMR (DMSO-d_6): δ 11.75 (Enol), 11.68 (Keto) (s,1H); 9.83 (Keto), 9.81 (Enol) (s,1H); 8.35 (Enol), 8.22 (Keto) (s, 1H); 8.32 – 8.29 (Enol and keto) (m, 1H); 8.02 (Enol and keto) (app dd, 1H); 7.45 – 7.37 (Enol and keto) (m, 2H); 7.13 – 7.10 (Enol and keto) (m, 1H); 2.28 (Keto), 2.02 (Enol) (s, 3H), ^{13}C NMR (DMSO-d_6): δ 172.4 (Keto), 166.0 (Enol) (C); 153.4 (Enol and keto) (C), 151.8 (Enol), 151.5 (Keto) (C); 145.8 (Enol), 143.1 (Keto) (CH); 138.1 (Enol and keto) (C); 136.5 (Enol and Keto) (CH); 128.8 (Enol), 128.7 (Keto) (CH); 128.2 (Enol), 128.1 (Keto) (C); 117.8 (Enol and keto) (CH); 117.6 (Enol), 117.3 (Keto) (CH); 112.2 (Enol), 112.1 (Keto) (CH); 21.8 (Enol), 20.3 (Keto) (CH). IR (KBr): ν(OH) 2928, ν(CO) 1678, ν(CN_{im}) 1594, ν(CN_{qui}) 1632, ρ(qui) 720 cm^{-1}. Suitable crystals for X-ray crystallography were grown by evaporation of an ethanol solution of 8-H_2QH.

2.2. Synthesis of 2-[(8-Hydroxyquinolinyl)methylene]hydrazinecarboxamide (8-H_2QS)

This compound has been previously synthesized as the hydrochloride salt.[58] Semicarbazide hydrochloride (0.123 g, 1.1 mmol) was dissolved in water (10 mL) and treated with an equivalent of sodium acetate (0.090 g, 1.1 mmol). A suspension of 8-hydroxy-2-quinolincarboxaldehyde (0.173 g, 1 mmol) in ethanol (10 mL) was added and the reaction mixture was refluxed for 4 h. The light yellow precipitate that formed was washed with water, ethanol and ether, air-dried and isolated in good yield (95%) and purity. Mp: 229.7 – 230.1 °C. Elemental Found (calcd) for $C_{11}H_{10}N_4O_2$: C, 57.74 (57.39); H 4.32 (4.38); N 23.87 (24.34). ^{1}H NMR (DMSO-d_6): δ 10.73 (s, 1H), 9.72 (s, 1H), 8.33 (d, *J* = 8.7 Hz, 1H), 8.25 (d, *J* = 8.7 Hz, 1H), 8.08 (s, 1H), 7.42 – 7.35 (m, 2H), 7.08 (dd, *J* = 1.4, 7.4 Hz, 1H), 6.74 (br s, 2H), ^{13}C NMR (DMSO-d_6): δ 156.5 (C), 153.2 (C), 152.2 (C), 139.8 (CH), 137.9 (C), 136.0 (CH), 128.5 (C), 127.7 (CH), 118.1

(CH), 117.7 (CH), 111.9 (CH). IR (KBr): ν(OH) 3152, ν(CO) 1720, ν(CN_{im}) 1572, ν(CN_{qui}) 1578, ρ(qui) 722 cm^{-1}.

2.3. Synthesis of copper complexes

2.3.1. Bis{2-[(8-Hydroxyquinolinyl)methylene]acetohydrazide}copper(II) Cu(8-HQH)$_2$

2-[(8-Hydroxyquinolinyl)methylene]acetohydrazide (0.344 g, 1.5 mmol) was dissolved in DMF (5 mL) and treated with an excess (0.359 g, 1.8 mmol) of $[Cu(OAc)_2]\cdot 2H_2O$. The reaction darkened considerably whilst stirring at room temperature for 4 h. Upon addition of water (5–10 mL) a solid precipitate was collected, washed repeatedly with water (3 x 5 mL) and dried *in vacuo* to afford a dark red solid (90 %). Elemental Found (calcd) for $C_{24}H_{20}N_6O_4Cu\cdot 0.5H_2O$: C, 54.89 (54.49); H, 4.01 (4.00); N, 15.86 (15.89). IR (KBr): ν(CO) 1674, ν(CN_{im}) 1586, ν(CN_{qui}) 1596, ρ(qui) 746, ν(MO) 540, ν(MN) 345 cm^{-1}. Effective magnetic moment = 1.66 (BM). MS (ES^+): m/z (calcd) 521.1011 (521.0140) [M + H^+].

2.3.2. Bis{2-[(8-Hydroxyquinolinyl)methylene]hydrazinecarboxamide}copper(II) Cu(8-HQS)$_2$

The reaction was carried out in a similar manner to Cu(8-HQH)$_2$ to afford a light green solid of Cu(8-HQS)$_2$ (99 %). Elemental Found (calcd) for $C_{22}H_{18}N_8O_4Cu\cdot 0.5H_2O$: C, 50.04 (49.76); H, 3.64 (3.61); N, 20.93 (21.10). IR (KBr): ν(CO) 1666, ν(CN_{im}) 1578, ν(CN_{qui}) 1556, ρ(qui) 756, ν(MO) 530, ν(MN) 476 cm^{-1}. Effective magnetic moment = 1.89 (BM). MS (ES^+): m/z (calcd) 523.0929 (522.9890) [M + H^+].

143 *2.3. Crystal structure determination*

144 Single-crystal X-ray diffraction measurements of 8-H_2QH were carried out on a
145 GEMINI-Ultra diffractometer (LabCri-UFMG) using graphite-Enhance Source Mo Kα
146 radiation (λ=0.71073 Å) at 150 K. Data collection, cell refinement results, and data
147 reduction were performed using the CRYSALISPRO software.[60] The semi-empirical
148 from equivalents absorption correction method was applied.[60] The structure was solved
149 by direct methods using SHELXS-97. Full-matrix least-squares refinement procedure
150 on F^2 with anisotropic thermal parameters was carried out using SHELXL-97.[61]
151 Positional and anisotropic atomic displacement parameters were refined for all non-
152 hydrogen atoms. Hydrogen atoms were placed geometrically and the positional
153 parameters were refined using a riding model. A molecular plot and crystal packing
154 figures were prepared using ORTEP[62] and MERCURY[63], respectively. Tables were
155 generated using WINGX suite.[64] A summary of the crystal data, data collection details
156 and refinement results are listed in Table 1.

157 ***Insert Table 1***

158 *2.4. Metal binding studies*

159 Metal binding studies were performed by varying the molar fractions of $CuCl_2$ from 0 to
160 1 (0 to 4.0 x 10^{-5} mol L^{-1}) in 20% DMSO/HEPES Buffer pH 7.4 in the presence of
161 ligand to obtain UV-Vis spectra. An absorbance maximum was assigned as interaction
162 of metal and ligand for each solution, which gave the determination of the metal:ligand
163 ratio in the complex.

164 *2.5. Calculations*

165 Density functional theory (DFT) calculations were used to obtain optimized geometries
166 for the doublet states of the Cu(8-HQH)$_2$, Cu(8-HQS)$_2$, Cu(CQ)$_2$, and Cu(8-QT)

complexes. The Gaussian 09 program (revision D.01)[65] was used with the B3LYP functional[66-67] and the 6-31G(d) basis set on all atoms. Frequency calculations at the same level of theory confirmed that the optimized structures were located at a minimum on the potential energy surface.

2.6. Determination of acidity constants by UV-Vis

The speciation of 8-H_2QS, 8-H_2QT and 8-H_2QH at physiological pH were obtained by the determination of acidity constants through variable pH UV-vis spectra. Solutions of 8-H_2QS, 8-H_2QT and 8-H_2QH (40 μM) were prepared in 5% DMSO in 0.1 M NaCl. A pH electrode was calibrated using a 2-point method (pH 4.01 and 10.01 standard buffers) before obtaining UV-Vis spectra. The pH of the ligand solutions was increased by NaOH to a starting point of ca. pH 12. UV-Vis spectra of the ligand solutions were obtained in the range of 600–190 nm at different pH by addition of aliquots of HCl. At least 30 UV-vis spectra were obtained in the range of pH 2–12. The HypSpec program (Protonic Software, UK) was used to analyze spectral data.[68] HySS2009 program (Protonic Software, UK) was used to simulate speciation diagrams for 8-H_2QS, 8-H_2QT and 8-H_2QH.[69]

2.7. Antioxidant capacity – TEAC test

The ability of the 8-hydroxyquinoline derivatives 8-H_2QH, 8-H_2QS and 8-H_2QT to scavenge free radicals was evaluated using the Trolox Equivalent Antioxidant Capacity (TEAC) assay.[70] These compounds were compared to both PBT2 and HCQ. Natural antioxidants, Vitamin E ((±)-α-tocopherol) and glutathione, were used as positive controls. The relative TEAC values were determined by a decolourization assay with 2,2′-azinobis(3-ethylbenzothiazoline-6-sulfonic acid (ABTS) radical cation. ABTS was dissolved in water (7 mM) and reacted with potassium persulfate (2.45 mM) in the dark

for 16 h to form the colored ABTS radical cation. This stock solution of ABTS was diluted with methanol to an absorbance value of 0.70 (± 0.02) at 744 nm. To start the reaction, solutions of 8-H_2QH, 8-H_2QS, 8-H_2QT, HCQ, and PBT2 in DMSO (20 μL, 3.0-15.0 μM) were added to 2 mL of ABTS solution. The absorbance value was measured in triplicate for each time point (1, 3, and 6 min). The value of absorbance at 744 nm was plotted as a function of compound concentration. The slopes were then compared to the standard, trolox (6-hydroxy-2,5,7,8-tetramethylchromane-2-carboxylic acid), with its TEAC value normalized to 1.[70-71]

2.8. Turbidity measurements

A 200 μM stock solution of lyophilized synthetic human $A\beta_{1–40}$ (21st Century Biochemicals) was freshly prepared before each trial was performed. Each vial of peptide, which contained *ca*. 0.25 mg $A\beta_{1–40}$, was dissolved in 290 μL of deionized water. To achieve complete dissolution of the peptide, sonication for 1 minute followed by a 30 second pause was repeated twice.[9] A 20 mM HEPES buffer solution containing 150 mM NaCl was prepared and treated with Chelex in deionized water at pH 6.6[72] and used to prepare stock solutions of ligands, Cu^{II}, and DTPA, as well as the reaction mixtures in the 96-well plates. The turbidity assay was conducted in quadruplicate in flat-bottomed 96-well assay plates (Microtest, BD Falcon). Ligands, Cu^{II} and $A\beta_{1–40}$ peptide had final concentrations of 150 μM, 25 μM and 25 μM, respectively. Cu^{II} solution was prepared from atomic absorption standards (Sigma-Aldrich). Cu^{II}, $A\beta_{1–40}$ and HEPES buffer were first added to the 96-well plate followed by the ligands. The solutions were incubated for 45 minutes at 37 °C under constant agitation, and each well in the 96-well plate was measured at 405 nm using a Synergy 4 Fluorometer plate reader from BioTek. Wells containing ligand, metal and buffer were used as blank and

subtracted from corresponding wells. Positive controls containing metal and peptide were used to demonstrate the effect of the absence of ligand on peptide aggregation.

2.9. Native Gel Electrophoresis and Western Blotting

$A\beta_{1-42}$ was first monomerized using a reported procedure, which includes dissolving $A\beta_{1-42}$ (21st Century Biochemicals) in hexafluoroisopropanol (HFIP) (0.5 mM), sonication for 15 min and incubating overnight at 4°C.[73-74] The solution was then aliquoted and evaporated under stream of N_2. The monomeric films were stored at -80 °C. The peptide was then dissolved in 1:1 DMSO/ddH_2O solution and concentration was assessed by UV-Vis spectroscopy. The amount of DMSO solvent (2.8%) in the eventual incubation solution is small, and has been previously shown to have no effect on fibril growth.[75] Aβ solutions were then incubated for 24 h at 37 °C with continuous agitation at 200 rpm to generate fibrils in the presence of ligands, or ligands and Cu^{II} in 0.1M PBS buffer at pH 7.4. A 10 – 20% gradient tris-tricine mini gel was used to separate samples at 100 V for 100 min at room temperature. The gels were transferred to a nitrocellulose membrane on an ice bath for 3 hours at 40 V at 4 °C. The membrane was blocked in a 3% BSA solution in TBS for 1 hour. The membrane was incubated in a solution (1:2000 dilution) of 6E10 anti-Aβ primary antibody (Covance) overnight at 298 K. After washing 4 X 15 mins with TBS buffer, the membrane was incubated in a solution containing the secondary antibody (Horseradish peroxidase, Caymen Chemicals) for 3 hours. Thermo Scientific SuperSignal® West Pico Chemiluminescent Substrate kit was used to visualize the Aβ species using a FUJIFILM Luminescent Image Analyzer (LAS-4000).

2.10. Transmission Electron Microscopy (TEM)

Samples were prepared from the Western blot assay after the 24 hour incubation time at 37 °C. TEM grids were prepared following previously reported methods.[9, 76] In order to increase hydrophilicity, the Formvar/Carbon 300-mesh grids (Electron Microscopy Sciences) were glow discharged in a vacuum for 15 seconds. Drops of samples (10 μL) were placed onto a sheet of parafilm and the TEM grid was laid on the drop for 5 minutes. The grid was then placed on the first drop of syringe-filtered 5% uranyl acetate and immediately removed, repeated for the second drop, then placed on the third drop to incubate for 1 minute. Excess uranyl acetate was removed using a tissue between drops. The grid was allowed to air-dry for at least 15 minutes. Bright field images were obtained on a Hitachi 8000 STEM with a lanthanum hexaboride thermoionic source operating at 200 kV and at a magnification of 20000 x.

2.11. Cytotoxic activity

2.11.1. Cell lines

HL60 (wild type human promyelocytic leukemia) and Jurkat (human immortalized line of T lymphocyte), cell lines were kindly donated by Dr. Gustavo Amarante-Mendes (Universidade de São Paulo, Brazil). MDA-MB 231 (human breast carcinoma) line was kindly provided by Dr. Alfredo Goes (Universidade Federal de Minas Gerais, Brazil). All lineages were maintained in the logarithmic phase of growth in RPMI 1640 or DMEM (Dulbecco's Modified Eagle Medium) supplemented with 100 U mL^{-1} penicillin and 100 mg mL^{-1} streptomycin (GIBCO BRL, Grand Island, NY) enriched with 2 mM of L-glutamine and 10% of fetal bovine serum (leukemic cells) or 5% (adherent cells). All cultures were maintained at 37 ºC in a humidified incubator with 5% CO_2 and 95% air. The media was changed twice a week and they were regularly examined.

2.11.2. Evaluation of the cytotoxic effect against human tumor cell lines

HL60 and Jurkat cells were inoculated at 50,000 and 100,000 cells/well, respectively, and MDA-MB cells were inoculated at 10,000 cells/well. The plates were pre-incubated for 24 h at 37 ºC to allow adaptation of cells prior to the addition of the test compounds. Freshly prepared solutions of the different compounds were tested at 10 μM. Subsequently, the plates were inoculated for 48 h in 5% CO_2 and 100% relative humidity atmosphere. Control groups included treatment with 0.5% DMSO (negative control) and 10 μM of cisplatin (positive control). Cell viability was estimated by measuring the rate of mitochondrial reduction of MTT.[77] All compounds were dissolved in DMSO prior to dilution. The optical densities (OD) were evaluated in a spectrophotometer at 595 nm. Controls included drug-containing medium (background) and drug-free complete medium. Drug-free complete medium was used as control (blank) and was treated in the same way as the drug-containing media. Results were expressed as percentage of cell proliferation, comparing with 0.5% DMSO control and were calculated as follows: viability (%) = (mean OD treated – mean OD background)/(mean OD untreated cultured, i.e. 0.5% DMSO – mean OD blank wells) x 100. Interactions of compounds and media were estimated on the basis of the variations between drug-containing medium and drug-free medium to minimize false-positive or false-negative readings.[78]

3. Results and discussion

3.1. Synthesis and Characterization

One new acetohydrazone ligand, 8-H_2QH, was synthesized by condensation of acethydrazide with 8-hydroxyquinoline-2-carboxaldehyde (Scheme 1). 8-H_2QS and 8-H_2QT have been previously prepared.[57-58] 8-H_2QH was characterized by elemental

analysis, which is in agreement with the proposed formula. The infrared spectrum (IR) of the hydrazone displays an absorption at 1678 cm^{-1}, which was assigned to ν(C=O), and the absorption at 1594 cm^{-1} was attributed to ν(C=N) of the iminic bond, confirming hydrazone formation.[79] Hydrazones have been reported to exist as tautomeric enolimines with the speciation dependent on electronic and structural effects, including inter- and intra-molecular hydrogen bonding.[80-81] Both the keto and enol forms were observed by ^{1}H NMR and ^{13}C NMR for 8-H_2QH in solution (Fig. S1). However, the X-ray crystallographic structural analysis indicates that in the solid state this compound exists only in the keto form.

Insert Scheme 1

3.2. Crystal Structure Determination

The ORTEP diagram of 8-H_2QH is shown in Fig. 2. Selected intramolecular bond lengths and angles, and hydrogen bonding parameters in the structure of 8-H_2QH are given in Tables S1 and S2 (Supporting Information), respectively. 8-H_2QH crystalizes with two independent molecules of the hydrazone (**A** and **B,** Fig. S2) per asymmetric unit. Since the geometrical parameters of the two molecules are similar (see Table 2 and S1), we will further describe molecule **A** here.

Insert Fig. 2

In **A** the C9–N2 and C10–O2 interatomic distances indicate double bond character (Table 2). The C=N–N–C(=O)C skeleton is almost planar (*rms* deviation from the least-squares plane of 0.0066 Å). The molecule adopts the *EE* conformation in relation to the C9–N2 and N3–C10 bonds, as indicated by the C2–C9=N2–N3, and N2–N3–C10–O2 torsion angles of 179.4(1) ^{o}, and 179.1(1) ^{o}, respectively.

Insert Table 2

In the molecular packing of 8-H_2QH various NH···O hydrogen bonds forming centrosymmetric dimers were observed. The NH···O and CH···O hydrogen bonds (see parameters in Table S2) involving **A** and **B** lead to the formation of an infinite two-dimensional (2D) network (Fig. S3). The low solubility of the compound may be attributed to these H-bonds as well as to π- π interactions in the solid state.

3.3. Ligand Speciation Studies

Speciation studies were performed in 5% DMSO in 0.1 M NaCl for 8-H_2QH, 8-H_2QS and 8-H_2QT in a range of pH varying from 2 to 12. In the pH range evaluated, there are four possible species (H_3L^+, H_2L, HL^-, L^{2-}, where H_2L is neutral) as shown in Scheme 2. Fitting the variable pH UV-Vis data for the compounds affords three pK_a values for each compound (Table 3), with the speciation diagrams shown in Fig. 3.

Insert Table 3

The pK_a values for HCQ have been reported as pK_{a1} 3.17 ± 0.11 and pK_{a2} 8.05 ± 0.08 at 25 °C.[82] The pK_{a1} refers to the deprotonation of the pyridine nitrogen and pK_{a2} refers to deprotonation of the hydroxyl oxygen. The pK_{a1} values for the 8-hydroxyquinoline derivatives studied are in accordance with the value reported in the literature for HCQ. The pK_{a1} value for 8-H_2QH is lower than those measured for 8-H_2QS and 8-H_2QT. 8-H_2QH displays a tautomeric equilibrium in solution (Fig. S1), that increases the electron-withdrawing effect of the hydrazone moiety on the quinoline scaffold. Consequently, the quinoline has its mesomeric stabilization also increased.[83] Electron-withdrawing groups, especially at position 2 of the quinoline, will decrease the electron density on the ring thus reducing the donating ability of the quinoline nitrogen atom.[84] The pK_{a2} values for 8-H_2QH, 8-H_2QS, and 8-H_2QT are higher than the value reported for HCQ. HCQ has two electron-withdrawing groups in the *o*- and *p*- positions (I and

Cl), which lowers the basicity of the quinoline hydroxyl.[83] Interestingly, the pK_{a3} value for 8-H_2QT is significantly less than the values for 8-H_2QH and 8-H_2QS. We attribute this difference to the stabilizing effect of the sulfur atom on the dianionic form of 8-H_2QT. This stabilizing effect likely plays a role in the different metal:ligand ratio in the Cu^{II} complex of 8-H_2QT in comparison to 8-H_2QH and 8-H_2QS (*vide infra*).

Insert Scheme 2

Insert Fig. 3

The *logK* n-octanol/water values ($logP_{calc}$, ALOGPS 2.1 software, Table 3) were calculated to evaluate the order of Gibbs free energies of solvation. The calculated values were not statistically different, suggesting equivalent solubility behavior in physiological fluids for all derivatives. However, evaluation of the absolute values of $logP_{calc}$ suggested a trend of hydrophobicity: 8-H_2QT > 8-H_2QH > 8-H_2QS. 8-H_2QT exhibited the lowest aqueous solubility in this work. The calculated values for HCQ are in accordance with the experimental data.[85] A similar trend obtained by the same software was previously validated for other Schiff-bases; the predicted $logP_{calc}$ values were similar to the experimental values but statistically different due to lower standard errors.[86]

3.3. Metal Binding Properties

UV-Vis spectroscopy was used to probe the solution binding of 8-H_2QS, 8-H_2QH and 8-H_2QT with Cu^{II}, and compare to the solid state characterization data. Changes in the intensity of the ligand-based transitions, along with the observation of new absorptions at ca. 449 nm and 438 nm indicated metal binding to ligand 8-H_2QH. Similar shifts of these peaks for 8-H_2QT and 8-H_2QS were also observed upon treatment with Cu^{II} indicating metal binding to the ligands. Job plot analysis (Fig. 4) suggests the formation

of a 1:1 metal:ligand compound for 8-H_2QT in agreement with previous reports of complex formation for this thiosemicarbazone and analogues.[56-57] Interestingly, a 1:2 metal:ligand ratio was determined for 8-H_2QS and 8-H_2QH with Cu^{II}, matching the solid-state characterization data for the complexes. The Job plot results, and resulting metal:ligand stoichiometries in solution, can be correlated to the pK_a values for the three ligands. The high pK_{a3} values for 8-H_2QS and 8-H_2QH (>12) suggest lower probability of deprotonation of the N–H Schiff base moiety leading to preferential formation of 1:2 metal:ligand complexes where only the phenolate has been deprotonated. On the other hand, the lower pK_{a3} value for the 8-H_2QT derivative leads to an increased stabilization of the dianionic form, inducing neutral 1:1 metal:ligand complex formation, with a tetradentate doubly deprotonated ligand. This proposition is in accordance to the presence of sulfur, a more polarizable atom in comparison to the oxygen atoms that are present in the 8-H_2QS and 8-H_2QH frameworks.

Insert Fig. 4

3.4. Theoretical Calculations of the Cu^{II} Complexes

We further investigated the Cu^{II} complexes of the 8-hydroxyquinoline ligands by theoretical calculations. A previously reported X-ray structure of Cu(8-QT) displays a 1:1 ligand:metal stoichiometry,[56] in accordance with our solution analysis (*vide supra*). The optimized geometry of Cu(8-QT) is in good agreement with the experimental metrical parameters, with coordination sphere bond lengths predicted within ± 0.06 Å (Fig. S5 and Table S3). Based on these results we employed the same functional and basis set to investigate the structures of Cu(8-HQH)$_2$ and Cu(8-HQS)$_2$, and compared the results to the reported 1:2 metal:ligand structure for Cu(CQ)$_2$.[87] The X-ray metricals for Cu(CQ)$_2$ and the computed values are shown in Table 4. The predicted coordination

sphere metrical parameters for Cu(8-HQH)$_2$, Cu(8-HQS)$_2$, and Cu(CQ)$_2$ are within ± 0.06 Å of the reported data for Cu(CQ)$_2$.[87] The computed structure of Cu(8-HQH)$_2$ is shown in Fig. 5, all other structures are shown in the Supporting Information (Fig. S5-S7). Of interest is the considerable distortion away from a square planar geometry predicted for both Cu(8-HQH)$_2$ and Cu(8-HQS)$_2$ (dihedral angle = 42° for both structures) in comparison to the reported structure for Cu(CQ)$_2$ (dihedral angle = 0°).[87] To further investigate the effects of crystal packing and steric interactions of the *o*-8-hydroxyquinoline substituents on the dihedral angle we calculated the optimized geometry of Cu(CQ)$_2$ at the same level of theory. The optimized geometry of Cu(CQ)$_2$ displays a dihedral angle of 17° (Fig. S7) which suggests that while crystal packing plays a role in flattening the reported Cu(CQ)$_2$ structure, the extended Schiff-base groups of the 8-H$_2$QH and 8-H$_2$QS ligands likely lead to the large predicted tetrahedral distortion observed for the corresponding 1:2 metal:ligand complexes.

Insert Fig. 5

Insert Table 4

3.5. Antioxidant Capacity – TEAC Test

Evidence of oxidative stress is widespread in AD, with early neuronal and pathological changes showing indications of oxidative damage.[88-89] The brain is particularly susceptible to oxidative damage due to the high rate of metabolic activity coupled with relatively low antioxidant levels and low tissue regenerative capacity.[31] We thus studied the antioxidant activity of 8-H$_2$QH, 8-H$_2$QS and 8-H$_2$QT via the Trolox Equivalent Antioxidant Capacity (TEAC) assay.[48, 70, 90] The ability of the compounds to quench the $ABTS^{\cdot+}$ radical cation was compared to Trolox, a water-soluble analog of (±)-α-tocopherol (Fig. 6). The Schiff-bases exhibited TEAC values that were statistically equivalent to (±)-α-tocopherol and enhanced in comparison to both PBT2 and HCQ.

The potent antioxidant properties observed for the Schiff-bases in this test in comparison to the other hydroxyquinoline derivatives is likely due to the negative inductive effect of the Cl and I ring substituents in PBT2 and HCQ which decrease the stability of a hydroxyl radical, reducing the antioxidant properties of these derivatives. In addition, the increased stabilization of the phenoxyl radical through the extended conjugation promoted by the semicarbazone, thiosemicarbazone and acetohydrazone moieties in the Schiff-bases may also contribute to the increased antioxidant properties of 8-H_2QH, 8-H_2QS, and 8-H_2QT.

Insert Fig. 6

3.6. Inhibition of Aβ Aggregation via Turbidity Measurements

A turbidity test was carried out as a preliminary evaluation of the ability of 8-hydroxyquinoline derivatives to modulate or even suppress the aggregation of the $A\beta_{1\text{-}40}$ peptide induced by Cu^{II}, providing information about the extent of peptide aggregation in solution on a short timescale (45 min). This test is completed by light scattering measurements at 405 nm.[9, 91] 8-H_2QT was not soluble under the test conditions (5% v/v DMSO in HEPES buffer pH 7.4), in agreement with its absolute $logP_{calc}$ value which suggests higher hydrophobicity in comparison to 8-H_2QH and 8-H_2QS. Therefore, the turbidity test was carried out for 8-H_2QH and 8-H_2QS. The pH value was adjusted to pH 6.6 to maximize the Cu^{II}-induced aggregation process.[9] Aggregation induced by Cu^{II} was significantly inhibited by compounds 8-H_2QH and 8-H_2QS with respect to the negative control (Cu^{II} and peptide) (Fig. 7). In addition, there was a statistically significant difference between 8-H_2QS and diethylenetriamine pentaacetic acid (DTPA, positive control) with respect to aggregation, suggesting that this derivative exhibits a greater inhibitory activity than the positive control under the test conditions; 8-H_2QH,

exhibits similar aggregation inhibition in comparison to DTPA. The higher anti-aggregating effect displayed by 8-H_2QS in comparison to 8-H_2QH in this test may be attributed to its higher hydrophilicity in comparison to 8-H_2QH (suggested by $logP_{calc}$ values), increased H-bonding interactions of the carboxamide function, and / or differences in the tautomeric ratio of the Schiff bases under the assay conditions.

Insert Fig.7

3.7. Monitoring Aβ Aggregation via Native Gel Electrophoresis and Western Blotting

It is possible to obtain a more detailed picture of the extent and pathways of Aβ aggregation by using native gel electrophoresis, Western blotting, and TEM analysis techniques. The lower molecular weight, soluble Aβ species can be visualized by native gel electrophoresis and Western blotting, while higher molecular weight and insoluble Aβ aggregates can be revealed by TEM analysis.[22] The aggregation process of the more neurotoxic and oligomer-forming[92-94] $A\beta_{1-42}$ peptide was probed by these aforementioned techniques in the presence of the 8-hydroxyquinoline compounds and Cu^{II}. Native gel electrophoresis and Western blotting and the corresponding TEM images are shown in Fig. 8. $A\beta_{1-42}$ was used at 25 μM for all the samples. Lane 2 contains $A\beta_{1-42}$ only, while Lanes 4, 6 and 8 contain $A\beta_{1-42}$ in the presence of 8-H_2QH, 8-H_2QS, and PBT2 respectively. The pattern of $A\beta_{1-42}$ aggregation does not change in the presence of 3 equiv. of the ligands showing that the ligands alone do not influence the aggregation process in this assay over 24 hrs. The pattern of $A\beta_{1-42}$ aggregation in the presence of Cu^{II} (1 equiv.) shows reduced aggregate formation (Lane 3), in accordance with prior reports of Cu^{II}-induced oligomer formation.[22, 24] Lanes 5, 7, and 9 contain, additionally to $A\beta_{1-42}$ and Cu^{II}, the ligands 8-H_2QH, 8-H_2QS and, PBT2

455 respectively. The addition of 8-H_2QH, 8-H_2QS, or PBT2 alters the pattern of
456 aggregation to match that of $A\beta_{1-42}$ only (Lane 2). These results suggest that the ligands
457 sequester Cu^{II}, likely restricting the formation of Cu^{II}-containing oligomers in this
458 assay. The TEM images are in accordance with the Gel assay, showing large molecular
459 weight aggregates for all Lanes except Lane 3 ($A\beta_{1-42}$ and Cu^{II}). Interestingly, the gel
460 assay for PBT2 (Lane 9) visually shows less large molecular weight aggregates in
461 comparison to both 8-H_2QH (Lane 5) and 8-H_2QS (Lane 7) suggesting that PBT2 does
462 not inhibit Cu^{II}-$A\beta_{1-42}$ peptide interactions to the same extent as the 8-H_2QX series.
463 While particle size analysis by TEM shows a range in sizes, certain trends are observed
464 in the data. The $A\beta_{1-42}$ only particle size range (0.12 – 68.99 μm^2) by TEM analysis is
465 larger than $A\beta_{1-42}$ in the presence of Cu^{II} (0.11 – 1.12 μm^2), in accordance with the gel
466 assay. $A\beta_{1-42}$ in the presence of Cu^{II} and 8-H_2QH (as an example ligand) shows
467 increased particle size (0.10 – 51.88 μm^2) in comparison to $A\beta_{1-42}$ and Cu^{II}, with data
468 similar to $A\beta_{1-42}$ alone. Full particle size analysis data is presented in Table S4.

469 ***Insert Fig. 8***

470 *3.8. Cytotoxic activity*

471 For the treatment of AD, to avoid undesirable side-effects, the compounds should
472 demonstrate low cytotoxicity. We investigated the preliminary cytotoxicity of 8-H_2QS
473 and 8-H_2QH in the MDA-MB, HL60, and Jurkat human tumor cell lines. A preliminary
474 screen (10 μM) of both compounds displayed very low cytotoxicity as measured by a
475 MTT assay.

476 ***Insert Table 5***

477 **4. Summary**

In the present work we synthesized and characterized a new acetohydrazone (8-H_2QH) derived from 8-hydroxyquinoline, its Cu^{II} complex and also the Cu^{II} complex of 8-hydroxyquinoline semicarbazone (8-H_2QS), as part of the evaluation of new metal-protein attenuating compounds (*MPAC*) as Alzheimer's disease (AD) therapeutics. The solution speciation (p*K*a values) suggest suitable physicochemical properties (neutral, water soluble) for CNS-targeting compounds, and the metal:ligand binding studies demonstrated the ability of the ligands to bind Cu^{II}, under physiological conditions. The antioxidant capacity of these ligands was tested, along with drug candidates PBT2 and HCQ. 8-H_2QH and 8-H_2QS displayed significantly higher antioxidant capacity when compared to PBT2 and HCQ. The chelating abilities of the Schiff-bases and their subsequent effects on amyloid-β peptide aggregation were evaluated. An initial turbidity assay with $A\beta_{1-40}$ was used to evaluate the influence of the ligands on the short-term Cu^{II}-induced aggregation of the peptide. 8-H_2QS, 8-H_2QH and DTPA (positive control) each presented a statistically significant decrease in aggregation in comparison to the negative control, $A\beta_{1-40}$ in the presence of Cu^{II}. Native gel electrophoresis/Western blotting and TEM images were used to evaluate the influence of the Schiff-base ligands and PBT2 on the aggregation of $A\beta_{1-42}$, both in the presence and absence of Cu^{II}. The Western blotting showed that the pattern of $A\beta_{1-42}$ aggregation in the presence of 8-H_2QH, 8-H_2QS, and PBT2 was similar to that of peptide only. The TEM results were in accordance with these observations. $A\beta_{1-42}$ in the presence of Cu^{II} showed a different pattern of aggregation, exhibiting the presence of oligomers (<15 KDa), while high molecular weight aggregates (>130 KDa) were inhibited. In the presence of 8-H_2QH or 8-H_2QS, and Cu^{II} the pattern of aggregation was similar to peptide only, suggesting that the Schiff-base ligands limit Cu^{II}-induced oligomer formation via metal complexation. A similar result was observed for PBT2, however

less high molecular weight aggregates were observed suggesting that this derivative does not restrict Cu^{II}-induced oligomer formation to the same extent as 8-H_2QH and 8-H_2QS in this assay. In summary, 8-H_2QH and 8-H_2QS were found to influence metal-induced Aβ aggregation and exhibit antioxidant capacity similar to vitamin E. Overall, the 8-hydroxiquinoline derivatives show promise for modulating metal-Aβ peptide interactions.

Abbreviations:

8-H_2QH	2-[(8-Hydroxyquinolinyl)methylene]acetohydrazide
8-H_2QS	2-[(8-Hydroxyquinolinyl)methylene]hydrazinecarboxamide
8-H_2QT	2-[(8-Hydroxyquinolinyl)methylene]hydrazinecarbothioamide
HQC	5-chloro-7-iodo-8-hydroxyquinoline (Clioquinol)
TEAC	Trolox Equivalent Antioxidant Capacity
TEM	Transmission Electron Microscopy
PBT2	5,7-dichloro-2-((dimethylanimo)methyl)quinolin-8-ol
ROS	reactive oxygen species
MPAC	Metal-Protein Attenuating Compounds
BBB	Blood-Brain Barrier
HEPES	4-(2-hydroxyethyl)-1-piperazineethanesulfonic acid
DFT	Density Functional Theory
ABTS	2,2′-azinobis(3-ethylbenzothiazoline-6-sulfonic acid
DTPA	Diethylene triamine pentaacetic acid
MTT	3-(4,5-dimethylthiazol-2-yl)-2,5-diphenyltetrazolium bromide

5. Acknowledgements

This work was supported by an NSERC Discovery Grant and a Michael Smith Career Investigator Award (to T.S.); Ciência sem Fronteiras (CNPq to R.P.V. and CAPES – Proc. n° 0711/13-6, Brazil to L.M.F.G.), Alzheimer Society of Canada for a doctoral award (to M.R.J.), International postdoctoral grant from the Swedish Research Council (Dnr:350-2012-239 to C.D.), Conselho Nacional de Desenvolvimento Científico e Tecnológico (CNPq, Brazil), INCT-INOFAR (Proc. CNPq 573.364/2008-6) and Fapemig. Westgrid and Compute Canada are thanked for access to computational resources.

6. References

1. E. Gaggelli, H. Kozlowski, D. Valensin, G. Valensin, Chem. Rev. 106 (2006) 1995-2044.

2. P.J. Crouch, K.J. Barnham, Acc. Chem. Res. 45 (2012) 1604-1611.

3. A.S. DeToma, S. Salamekh, A. Ramamoorthy, M.H. Lim, Chem. Soc. Rev. 41 (2012) 608-621.

4. A. Budimir, Acta Pharmaceut 61 (2011) 1-14.

5. Dementia cases set to triple by 2050 but still largely ignored. http://www.who.int/mediacentre/news/releases/2012/dementia_20120411/en/ (accessed 12 december 2013).

6. C. Rodriguez-Rodriguez, M. Telpoukhovskaia, C. Orvig, Coord. Chem. Rev. 256 (2012) 2308-2332.

7. S. Lee, X. Zheng, J. Krishnamoorthy, M.G. Savelieff, H.M. Park, J.R. Brender, J.H. Kim, J.S. Derrick, A. Kochi, H.J. Lee, C. Kim, A. Ramamoorthy, M.T. Bowers, M.H. Lim, J. Am. Chem. Soc. (2014).

8. V.H. Finder, J. Alzheimers Dis. 22 (2010) S5-S19.

9. M.R. Jones, E.L. Service, J.R. Thompson, M.C. Wang, I.J. Kimsey, A.S. DeToma, A. Ramamoorthy, M.H. Lim, T. Storr, Metallomics 4 (2012) 910-20.

10. M.P. Mazanetz, P.M. Fischer, Nature Rev. Drug. Disc. 6 (2007) 464-479.

11. A. Abbott, Nature 456 (2008) 161-164.

12. J. Hardy, D.J. Selkoe, Science 297 (2002) 353-356.

13. D.J. Selkoe, Nature Medicine 17 (2011) 1693-1693.

14. S. Lesne, M.T. Koh, L. Kotilinek, R. Kayed, C.G. Glabe, A. Yang, M. Gallagher, K.H. Ashe, Nature 440 (2006) 352-357.

15. A. Lakatos, B. Gyurcsik, N.V. Nagy, Z. Csendes, E. Weber, L. Fulop, T. Kiss, Dalton Trans. 41 (2012) 1713-1726.

16. S.L. Leong, T.R. Young, K.J. Barnham, A.G. Wedd, M.G. Hinds, Z. Xiao, R. Cappai, Metallomics 6 (2014) 105-116.

17. A.S. Pithadia, A. Kochi, M.T. Soper, M.W. Beck, Y.Z. Liu, S. Lee, A.S. DeToma, B.T. Ruotolo, M.H. Lim, Inorg. Chem. 51 (2012) 12959-12967.

18. F. Bousejra-ElGarah, C. Bijani, Y. Coppel, P. Faller, C. Hureau, Inorg. Chem. 50 (2011) 9024-9030.

19. A.I. Bush, W.H. Pettingell, G. Multhaup, M.d. Paradis, J.-P. Vonsattel, J.F. Gusella, K. Beyreuther, C.L. Masters, R.E. Tanzi, Science 265 (1994) 1464-7.

20. C.S. Atwood, R.D. Moir, X. Huang, R.C. Scarpa, N.M. Bacarra, D.M. Romano, M.A. Hartshorn, R.E. Tanzi, A.I. Bush, J. Biol. Chem. 273 (1998) 12817-26.

21. X.D. Huang, C.S. Atwood, R.D. Moir, M.A. Hartshorn, R.E. Tanzi, A.I. Bush, J. Biol. Inorg. Chem. 9 (2004) 954-960.

22. A.K. Sharma, S.T. Pavlova, J. Kim, J. Kim, L.M. Mirica, Metallomics 5 (2013) 1529-1536.

23. R.R. Crichton, D.T. Dexter, R.J. Ward, Coord. Chem. Rev. 252 (2008) 1189-1199.

24. A.D. Watt, V.L. Villemagne, K.J. Barnham, J. Alzheimers Dis. 33 Suppl 1 (2013) S283-93.

25. C.A. McLean, R.A. Cherny, F.W. Fraser, S.J. Fuller, M.J. Smith, K. Beyreuther, A.I. Bush, C.L. Masters, Ann. Neurol. 46 (1999) 860-866.

26. Y. Yoshiike, K. Tanemura, O. Murayama, T. Akagi, M. Murayama, S. Sato, X. Sun, N. Tanaka, A. Takashima, New insights on how metals disrupt amyloid .beta.-

aggregation and their effects on amyloid-.beta. cytotoxicity. In J. Biol. Chem., 2001; Vol. 276, pp 32293-32299.

27. C. Exley, Coord. Chem. Rev. 256 (2012) 3114-3114.

28. M. Mold, L. Ouro-Gnao, B.M. Wieckowski, C. Exley, Sci. Rep. 3 (2013) 1256.

29. A.K. Sharma, S.T. Pavlova, J. Kim, D. Finkelstein, N.J. Hawco, N.P. Rath, J. Kim, L.M. Mirica, J. Am. Chem. Soc. 134 (2012) 6625-6636.

30. S.R. Bareggi, U. Cornelli, CNS Neurosci Ther 18 (2012) 41-46.

31. K.J. Barnham, C.L. Masters, A.I. Bush, Nature Rev. Drug. Disc. 3 (2004) 205-214.

32. A.R. White, T. Du, K.M. Laughton, I. Volitakis, R.A. Sharples, M.E. Xilinas, D.E. Hoke, R.M.D. Holsinger, G. Evin, R.A. Cherny, A.F. Hill, K.J. Barnham, Q.X. Li, A.I. Bush, C.L. Masters, J. Biol. Chem. 281 (2006) 17670-17680.

33. P.J. Crouch, L.W. Hung, P.A. Adlard, M. Cortes, V. Lal, G. Filiz, K.A. Perez, M. Nurjono, A. Caragounis, T. Du, K. Laughton, I. Volitakis, A.I. Bush, Q.X. Li, C.L. Masters, R. Cappai, R.A. Cherny, P.S. Donnelly, A.R. White, K.J. Barnham, Proc. Natl. Acad. Sci. U. S. A. 106 (2009) 381-386.

34. P.J. Crouch, M.S. Savva, L.W. Hung, P.S. Donnelly, A.I. Mot, S.J. Parker, M.A. Greenough, I. Volitakis, P.A. Adlard, R.A. Cherny, C.L. Masters, A.I. Bush, K.J. Barnham, A.R. White, J. Neurochem. 119 (2011) 220-230.

35. R.A. Cherny, C.S. Atwood, M.E. Xilinas, D.N. Gray, W.D. Jones, C.A. McLean, K.J. Barnham, I. Volitakis, F.W. Fraser, Y.S. Kim, X.D. Huang, L.E. Goldstein, R.D. Moir, J.T. Lim, K. Beyreuther, H. Zheng, R.E. Tanzi, C.L. Masters, A.I. Bush, Neuron 30 (2001) 665-676.

36. C.W. Ritchie, A.I. Bush, A. Mackinnon, S. Macfarlane, M. Mastwyk, L. MacGregor, L. Kiers, R. Cherny, Q.-X. Li, A. Tammer, D. Carrington, C. Mavros, I.

Volitakis, M. Xilinas, D. Ames, S. Davis, K. Beyreuther, R.E. Tanzi, C.L. Masters, Arch. Neurol. 60 (2003) 1685-1691.

37. A.I. Bush, J. Alzheimers Dis. 15 (2008) 223-240.

38. P.A. Adlard, R.A. Cherny, D.I. Finkelstein, E. Gautier, E. Robb, M. Cortes, I. Volitakis, X. Liu, J.P. Smith, K. Perez, K. Laughton, Q.X. Li, S.A. Charman, J.A. Nicolazzo, S. Wilkins, K. Deleva, T. Lynch, G. Kok, C.W. Ritchie, R.E. Tanzi, R. Cappai, C.L. Masters, K.J. Barnham, A.I. Bush, Neuron 59 (2008) 43-55.

39. N.G. Faux, C.W. Ritchie, A. Gunn, A. Rembach, A. Tsatsanis, J. Bedo, J. Harrison, L. Lannfelt, K. Blennow, H. Zetterberg, M. Ingelsson, C.L. Masters, R.E. Tanzi, J.L. Cummings, C.M. Herd, A.I. Bush, J. Alzheimers Dis. 20 (2010) 509-516.

40. L. Lannfelt, K. Blennow, H. Zetterberg, S. Batsman, D. Ames, J. Hrrison, C.L. Masters, S. Targum, A.I. Bush, R. Murdoch, J. Wilson, C.W. Ritchie, P.E.S. Grp, Lancet Neurol. 7 (2008) 779-786.

41. D.R. Crapper McLachlan, A.J. Dalton, T.P. Kruck, M.Y. Bell, W.L. Smith, W. Kalow, D.F. Andrews, Lancet 337 (1991) 1304-8.

42. J.-S. Choi, J.J. Braymer, R.P.R. Nanga, A. Ramamoorthy, M.H. Lim, Proc. Natl. Acad. Sci. U. S. A. 107 (2010) 21990-21995.

43. R.A. Cherny, J.T. Legg, C.A. McLean, D.P. Fairlie, X. Huang, C.S. Atwood, K. Beyreuther, R.E. Tanzi, C.L. Masters, A.I. Bush, J. Biol. Chem. 274 (1999) 23223-8.

44. S.-J. Hyung, A.S. DeToma, J.R. Brender, S. Lee, S. Vivekanandan, A. Kochi, J.-S. Choi, A. Ramamoorthy, B.T. Ruotolo, M.H. Lim, Proc. Natl. Acad. Sci. U. S. A. 110 (2013) 3743-3748.

45. M.A. Telpoukhovskaia, C. Orvig, Chem. Soc. Rev. 42 (2013) 1836-1846.

46. L.E. Scott, M. Telpoukhovskaia, C. Rodriguez-Rodriguez, M. Merkel, M.L. Bowen, B.D.G. Page, D.E. Green, T. Storr, F. Thomas, D.D. Allen, P.R. Lockman, B.O. Patrick, M.J. Adam, C. Orvig, Chem. Sci. 2 (2011) 642-648.

47. K.J. Franz, Curr. Opin. Chem. Biol. 17 (2013) 143-149.

48. T. Storr, M. Merkel, G.X. Song-Zhao, L.E. Scott, D.E. Green, M.L. Bowen, K.H. Thompson, B.O. Patrick, H. Schugar, C. Orvig, J. Am. Chem. Soc. 129 (2007) 7453-7463.

49. H. Beraldo, D. Gambino, Mini Rev Med Chem 4 (2004) 31-9.

50. Y. Yu, J. Wong, D.B. Lovejoy, D.S. Kalinowski, D.R. Richardson, Clin. Cancer Res. 12 (2006) 6876-83.

51. T.B. Chaston, D.B. Lovejoy, R.N. Watts, D.R. Richardson, Clin. Cancer Res. 9 (2003) 402-14.

52. J. Shao, B. Zhou, A.J. Di Bilio, L. Zhu, T. Wang, C. Qi, J. Shih, Y. Yen, Mol. Cancer Ther. 5 (2006) 586-92.

53. C.E. Cooper, G.R. Lynagh, K.P. Hoyes, R.C. Hider, R. Cammack, J.B. Porter, J. Biol. Chem. 271 (1996) 20291-9.

54. S. Nyholm, G.J. Mann, A.G. Johansson, R.J. Bergeron, A. Graslund, L. Thelander, J. Biol. Chem. 268 (1993) 26200-5.

55. V.M. Nelson, C.M. Dancik, W. Pan, Z.G. Jiang, M.S. Lebowitz, H.A. Ghanbari, J. Alzheimers Dis. 17 (2009) 611-9.

56. J.L. Hickey, P.J. Crouch, S. Mey, A. Caragounis, J.M. White, A.R. White, P.S. Donnelly, Dalton Trans. 40 (2011) 1338-1347.

57. H. Zhang, R. Thomas, D. Oupicky, F. Peng, J. Biol. Inorg. Chem. 13 (2008) 47-55.

58. M. Albrecht, O. Osetska, R. Frohlich, Dalton Trans. (2005) 3757-3762.

59. K.J. Barnham, E.C.L. Gautier, G.B. Kok, G.W. Krippner 8-Hydroxi quinoline derivatives. WO 2004007461, 2008.

60. CrysAlis171.NET CRYSALISPRO, 1.171.35.15 Oxford Diffraction, Ltd.: Wembly, Middlesex, U.K., 2011.

61. G.M. Sheldrick, Acta Crystallogr A 64 (2008) 112-122.

62. L.J. Farrugia, J. Appl. Crystallogr. 30 (1997) 568.

63. C.F. Macrae, I.J. Bruno, J.A. Chisholm, P.R. Edgington, P. McCabe, E. Pidcock, L. Rodriguez-Monge, R. Taylor, J. van de Streek, P.A. Wood, J. Appl. Crystallogr. 41 (2008) 466-470.

64. L.J. Farrugia, J. Appl. Crystallogr. 32 (1999) 837-838.

65. M.J. Frisch, G.W. Trucks, H.B. Schlegel, G.E. Scuseria, M.A. Robb, J.R. Cheeseman, G. Scalmani, V. Barone, B. Mennucci, G.A. Petersson, H. Nakatsuji, M. Caricato, X. Li, H.P. Hratchian, A.F. Izmaylov, J. Bloino, G. Zheng, J.L. Sonnenberg, M. Hada, M. Ehara, K. Toyota, R. Fukuda, J. Hasegawa, M. Ishida, T. Nakajima, Y. Honda, O. Kitao, H. Nakai, T. Vreven, J. Montgomery, J. A. , J.E. Peralta, F. Ogliaro, M. Bearpark, J.J. Heyd, E. Brothers, K.N. Kudin, V.N. Staroverov, R. Kobayashi, J. Normand, K. Raghavachari, A. Rendell, J.C. Burant, S.S. Iyengar, J. Tomasi, M. Cossi, N. Rega, N.J. Millam, M. Klene, J.E. Knox, J.B. Cross, V. Bakken, C. Adamo, J. Jaramillo, R. Gomperts, R.E. Stratmann, O. Yazyev, A.J. Austin, R. Cammi, C. Pomelli, J.W. Ochterski, R.L. Martin, K. Morokuma, V.G. Zakrzewski, G.A. Voth, P. Salvador, J.J. Dannenberg, S. Dapprich, A.D. Daniels, Ö. Farkas, J.B. Foresman, J.V. Ortiz, J. Cioslowski, D.J. Fox, Gaussian 09, Revision A.02. Gaussian, Inc., Wallingford, CT, 2009.

66. A.D. Becke, J. Chem. Phys. 98 (1993) 5648-5652.

67. P.J. Stephens, F.J. Devlin, C.F. Chabalowski, M.J. Frisch, J. Phys. Chem. 98 (1994) 11623-11627.

68. P. Gans, A. Sabatini, A. Vacca, Ann Chim-Rome 89 (1999) 45-49.

69. L. Alderighi, P. Gans, A. Ienco, D. Peters, A. Sabatini, A. Vacca, Coord. Chem. Rev. 184 (1999) 311-318.

70. R. Re, N. Pellegrini, A. Proteggente, A. Pannala, M. Yang, C. Rice-Evans, Free Radic. Biol. Med. 26 (1999) 1231-7.

71. T. Storr, L.E. Scott, M.L. Bowen, D.E. Green, K.H. Thompson, H.J. Schugar, C. Orvig, Dalton Trans (2009) 3034-43.

72. M. Sokolowska, W. Bal, J. Inorg. Biochem. 99 (2005) 1653-1660.

73. R. Sabate, M. Gallardo, J. Estelrich, Biopolymers 71 (2003) 190-5.

74. S.K. Pachahara, N. Chaudhary, C. Subbalakshmi, R. Nagaraj, J. Pept. Sci. 18 (2012) 233-41.

75. C.L. Shen, R.M. Murphy, Biophys. J. 69 (1995) 640-651.

76. A.M. Mancino, S.S. Hindo, A. Kochi, M.H. Lim, Inorg. Chem. 48 (2009) 9596-9598.

77. T. Mosmann, J. Immunol. Methods 65 (1983) 55-63.

78. A. Monks, D. Scudiero, P. Skehan, R. Shoemaker, K. Paull, D. Vistica, C. Hose, J. Langley, P. Cronise, A. Vaigro-Wolff, et al., J. Natl. Cancer Inst. 83 (1991) 757-66.

79. G.L. Parrilha, R.P. Vieira, A.P. Rebolledo, I.C. Mendes, L.M. Lima, E.J. Barreiro, O.E. Piro, E.E. Castellano, H. Beraldo, Polyhedron 30 (2011) 1891-1898.

80. N. Galic, B. Peric, B. Kojic-Prodic, Z. Cimerman, J. Mol. Struct. 559 (2001) 187-194.

81. G.C. Xu, L. Zhang, L. Liu, G.F. Liu, D.Z. Jia, Polyhedron 27 (2008) 12-24.

82. H. Tanaka, Z. Tamura, J. Pharm. Sci. 73 (1984) 1647-9.

83. P. Sykes, A guidebook to mechanism in organic chemistry. Sixth ed., Longman Scientific & Technical, Cambridge 1985, Vol. 1, p 416.

84. I. Novak, B. Kovac, J. Org. Chem. 69 (2004) 5005-10.

85. H. Tanaka, Z. Tamura, J. Pharm. Sci. 73 (1984) 1647-1649.

86. R.P. Vieira, J.A. Lessa, W.C. Ferreira, F.B. Costa, L.F. Bastos, W.R. Rocha, M.M. Coelho, H. Beraldo, Eur. J. Med. Chem. 50 (2012) 140-8.

87. M. Di Vaira, C. Bazzicalupi, P. Orioli, L. Messori, B. Bruni, P. Zatta, Inorg. Chem. 43 (2004) 3795-3797.

88. A. Nunomura, G. Perry, G. Aliev, K. Hirai, A. Takeda, E.K. Balraj, P.K. Jones, H. Ghanbari, T. Wataya, S. Shimohama, S. Chiba, C.S. Atwood, R.B. Petersen, M.A. Smith, J. Neuropathol. Exp. Neurol. 60 (2001) 759-767.

89. D.H. Cho, T. Nakamura, J.G. Fang, P. Cieplak, A. Godzik, Z. Gu, S.A. Lipton, Science 324 (2009) 102-105.

90. M.G. Savelieff, Y. Liu, R.R. Senthamarai, K.J. Korshavn, H.J. Lee, A. Ramamoorthy, M.H. Lim, Chem. Commun. (2014) ASAP.

91. T. Storr, M. Merkel, G.X. Song-Zhao, L.E. Scott, D.E. Green, M.L. Bowen, K.H. Thompson, B.O. Patrick, H.J. Schugar, C. Orvig, J. Am. Chem. Soc. 129 (2007) 7453-7463.

92. D.M. Walsh, D.J. Selkoe, J. Neurochem. 101 (2007) 1172-1184.

93. C. Haass, D.J. Selkoe, Nat. Rev. Mol. Cell Biol. 8 (2007) 101-112.

94. Y.S. Gong, L. Chang, K.L. Viola, P.N. Lacor, M.P. Lambert, C.E. Finch, G.A. Krafft, W.L. Klein, Proc. Natl. Acad. Sci. U. S. A. 100 (2003) 10417-10422.

95. I.V. Tetko, J. Gasteiger, R. Todeschini, A. Mauri, D. Livingstone, P. Ertl, V. Palyulin, E. Radchenko, N.S. Zefirov, A.S. Makarenko, V.Y. Tanchuk, V.V. Prokopenko, J. Comput. Aided Mol. Des. 19 (2005) 453-463.

96. (2005).

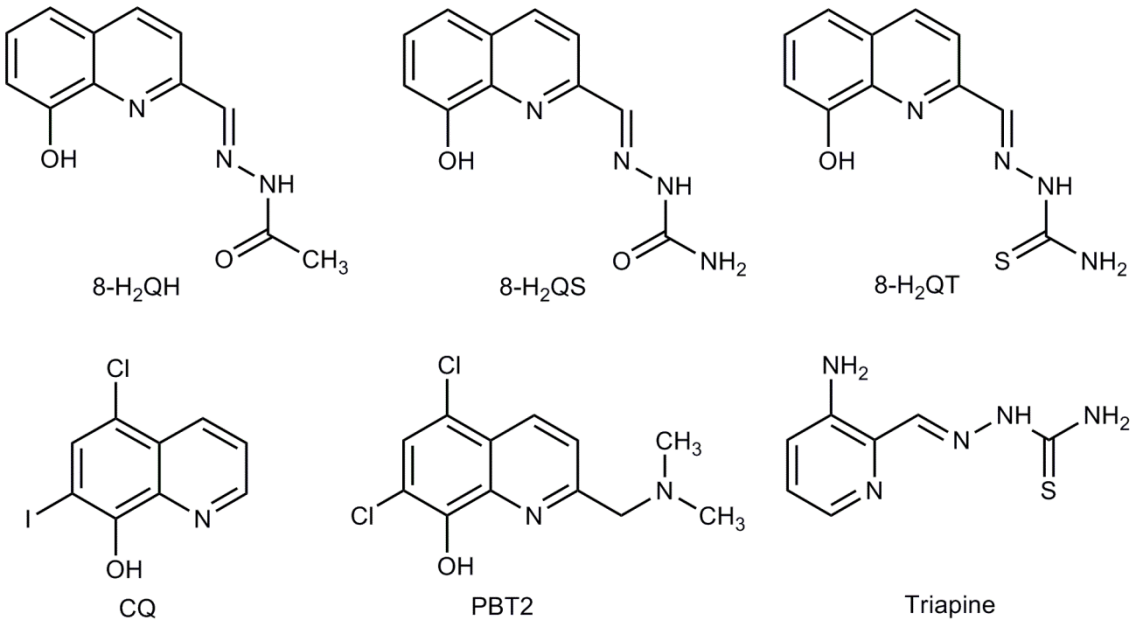

Figure 1. Chemical structures of 2-[(8-Hydroxyquinolinyl)methylene]acetohydrazide (8-H_2QH), 2-[(8-Hydroxyquinolinyl)methylene]hydrazinecarboxamide (8-H_2QS), 2-[(8-Hydroxyquinolinyl)methylene]hydrazinecarbothioamide (8-H_2QT), Clioquinol (HCQ), PBT2, and Triapine.

Table 1. Crystal structure and refinement data for 8-H_2QH.

Compound		8-H_2QH
Empirical Formula		$C_{12}H_{11}N_3O_2$
Formula Weight		229.24
Temperature, K		150(2)
Wavelength, Å		0.71073
Crystal System		Triclinic
Space Group		Pī
Unit cell dimensions	a, Å	8.6542(2)
	b, Å	10.2904(4)
	c, Å	12.6933(4)
	α, º	72.860(3)
	β, º	83.873(2)
	γ, º	87.479(2)
Volume, Å^3		1073.94(6)
Z / Density calc., Mg/m^3		4 / 1.418
Absorption coefficient, mm^{-1}		0.100
Reflection collect. / unique [R_{int}]		23880/ 4390 [R(int) = 0.0268]
Goodness–of–fit on F^2		1.055
R indices (all data)		R1 = 0.0363, wR2 = 0.1005
Final R indices [I>2σ(I)]		R1 = 0.0423, wR2 = 0.1079

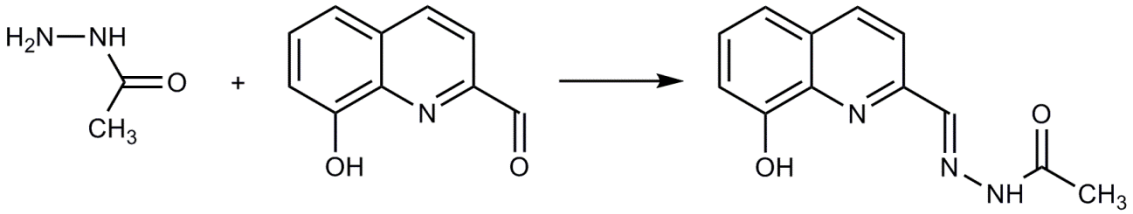

Scheme 1. Synthesis of 8-H_2QH. The keto form is shown.

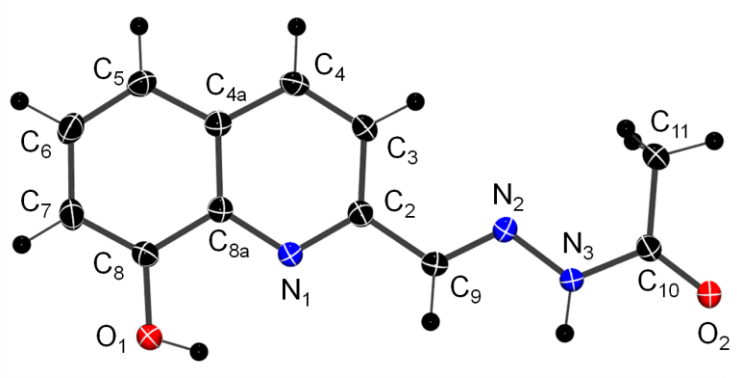

Figure 2. ORTEP diagram for 8-H_2QH with thermal ellipsoids at the 50% probability level. Hydrogen atoms are drawn as circles of arbitrary radii.

Table 2. Selected bond lengths (Å) and torsion angles (^{o}) for the 8-H_2QH structure.

Bond (Å)		Angles (^{o})	
N1–C2	1.328(2)	O1–C8–C8A	118.0(1)
C2–C9	1.464(2)	C8–C8A–N1	116.5(1)
C9–N2	1.280(2)	N1–C2–C9	115.7(1)
N2–N3	1.363(2)	C2–C9–N2	119.8(1)
N3–C10	1.358(2)	C9–N2–N3	116.5(1)
C10–O2	1.230(2)	N2–N3–C10	120.3(1)
C10–C11	1.503(2)	N3–C10–O2	119.8(1)
C8–O1	1.358(2)	N3–C10–C11	122.9(1)

Table 3. pK_a and logP_{calc} values of compounds 8-H_2QT, 8-H_2QH and 8-H_2QS. pK_a data were analyzed using the HypSpec program (Protonic Software, UK), and logP_{calc} was calculated using ALOGPS 2.1 software.[95,96]

Compound	pK_{a1}	pK_{a2}	pK_{a3}	logP_{calc}	logP_{exp}
8-H_2QT	3.36 ± 0.01	9.51 ± 0.01	11.75 ± 0.01	1.67 ± 0.31	-
8-H_2QH	2.87 ± 0.03	9.53 ± 0.03	13.50 ± 0.01	1.62 ± 0.58	-
8-H_2QS	3.25 ± 0.02	9.63 ± 0.01	13.16 ± 0.01	1.12 ± 0.29	-
HCQ[a]	3.17 ± 0.11	8.05 ± 0.08	-	3.43 ± 0.21	3.24[a]

[a][82]

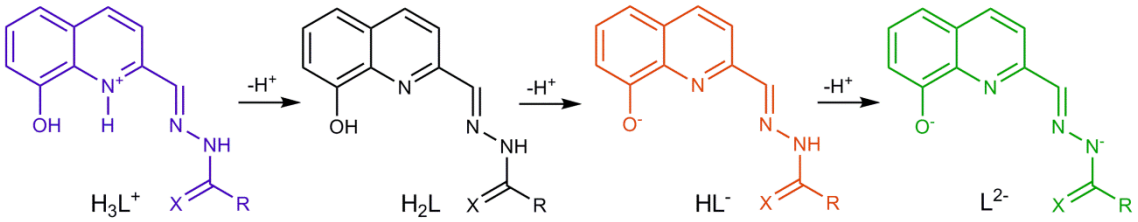

Scheme 2. Protonation states of the 8-hydroxyquinoline Schiff-base ligands.

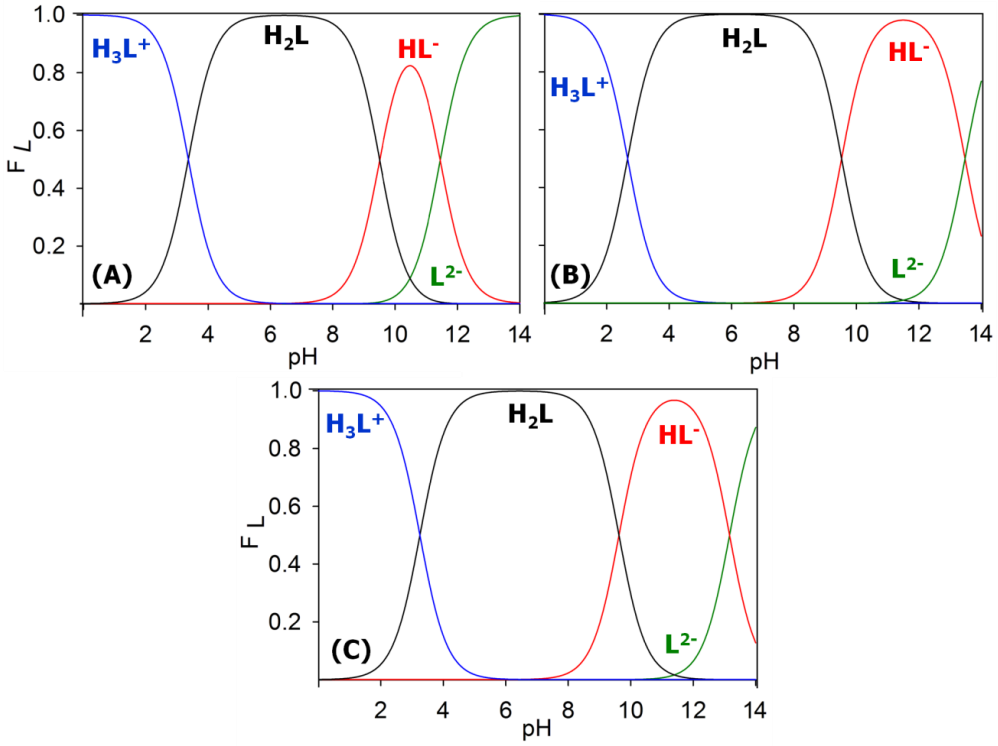

Figure 3. Speciation diagrams of 8-H_2QT (**A**), 8-H_2QH (**B**) and 8-H_2QS (**C**). F_L = fraction of species. H_2L = neutral species. Diagrams were simulated using the HySS2009 program (Protonic Software, UK).

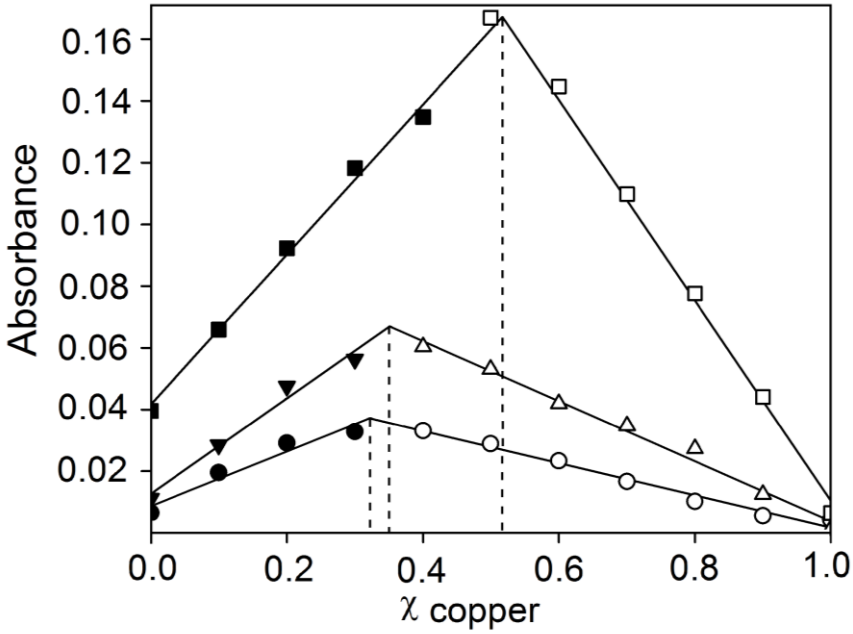

Figure 4. Job plots of 8-H_2QS (▼ / Δ 420 nm), 8-H_2QH (● / ○ 449 nm) and 8-H_2QT (■ / □ 404 nm) with copper acetate (20% DMSO in HEPES buffer pH 7.4). The dashed lines for 8-H_2QH ($\chi = 0.33$ Cu^{II}) and 8-H_2QS ($\chi = 0.35$ Cu^{II}) indicate a 1:2 Cu^{II}:L stoichiometry. The dashed line for 8-H_2QT ($\chi = 0.52$ Cu^{II}) indicates a 1:1 Cu^{II}:L stoichiometry.

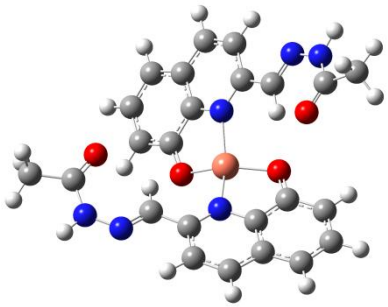

Figure 5. DFT-optimized geometry of Cu(8-HQH)$_2$ displaying a distorted square planar geometry with a metal coordination sphere torsion angle of 47^o. See Experimental Section for calculation details.

Table 4. Comparison of experimental ($Cu(CQ)_2$) and calculated ($Cu(8\text{-}HQH)_2$, $Cu(8\text{-}HQS)_2$, $Cu(CQ)_2$) coordination sphere bond lengths. See Experimental Section for calculation details.

	Experimental (Å)[a]	Predicted Bond Lengths (Å)		
	$Cu(CQ)_2$	$Cu(CQ)_2$	$Cu(8\text{-}HQH)_2$	$Cu(8\text{-}HQS)_2$
Cu – N1	1.984	1.969	2.016	2.017
Cu – N2	1.963	1.969	2.016	2.017
Cu – O1	1.915	1.904	1.888	1.887
Cu – O2	1.923	1.904	1.888	1.887

[a][87]

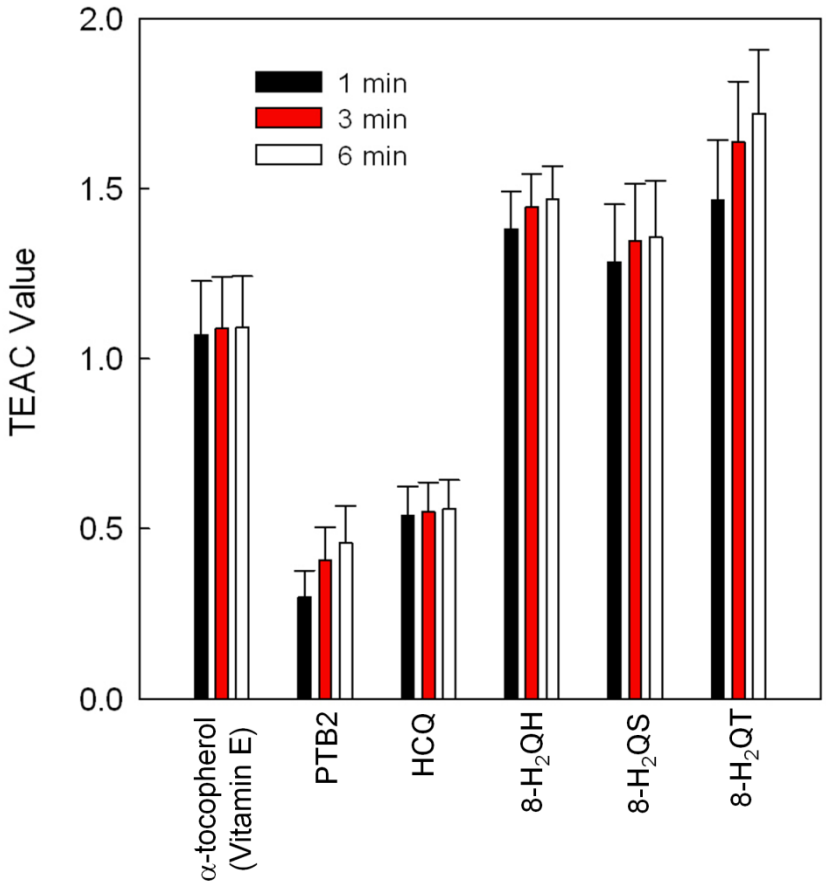

Figure 6. Trolox Equivalent Antioxidant Capacity (TEAC) values at 1, 3, and 6 min for (±)-α-tocopherol, PBT2, Clioquinol (HCQ), 8-H_2QH, 8-H_2QS and 8-H_2QT. Error bars represent ± SD above and below the average TEAC value (determined in triplicate).

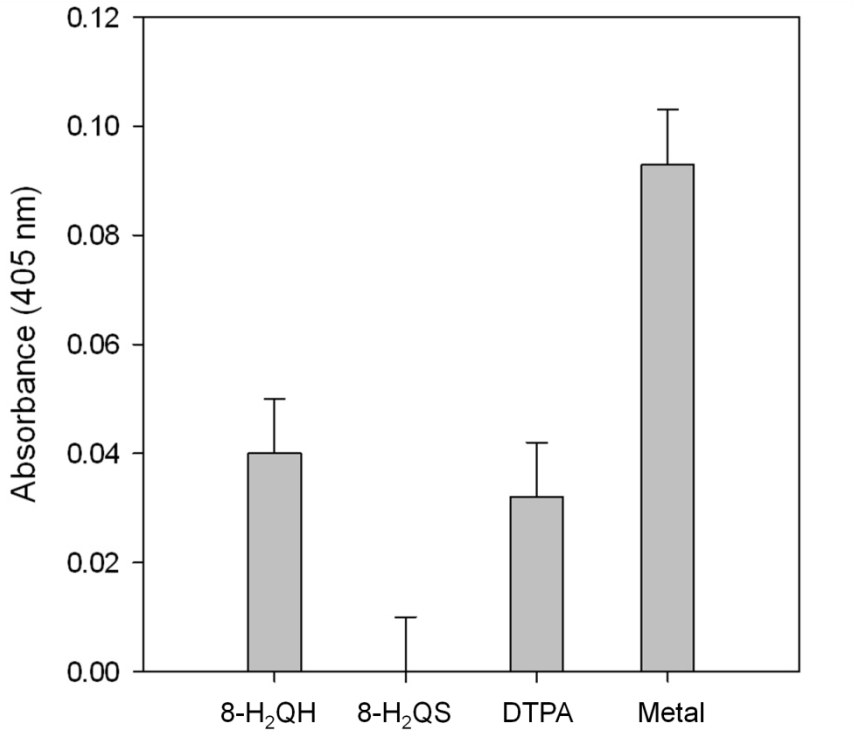

Figure 7. Degree of $A\beta_{1–40}$ aggregation as measured by UV-Vis measurements. Data represent the mean absorbance of quadruplicate trials at 405 nm of peptide in the presence of Cu^{II} ions, and Cu^{II} and ligands at pH 6.6. Error bars represent ± SD above (and below not shown) the average absorbance value.

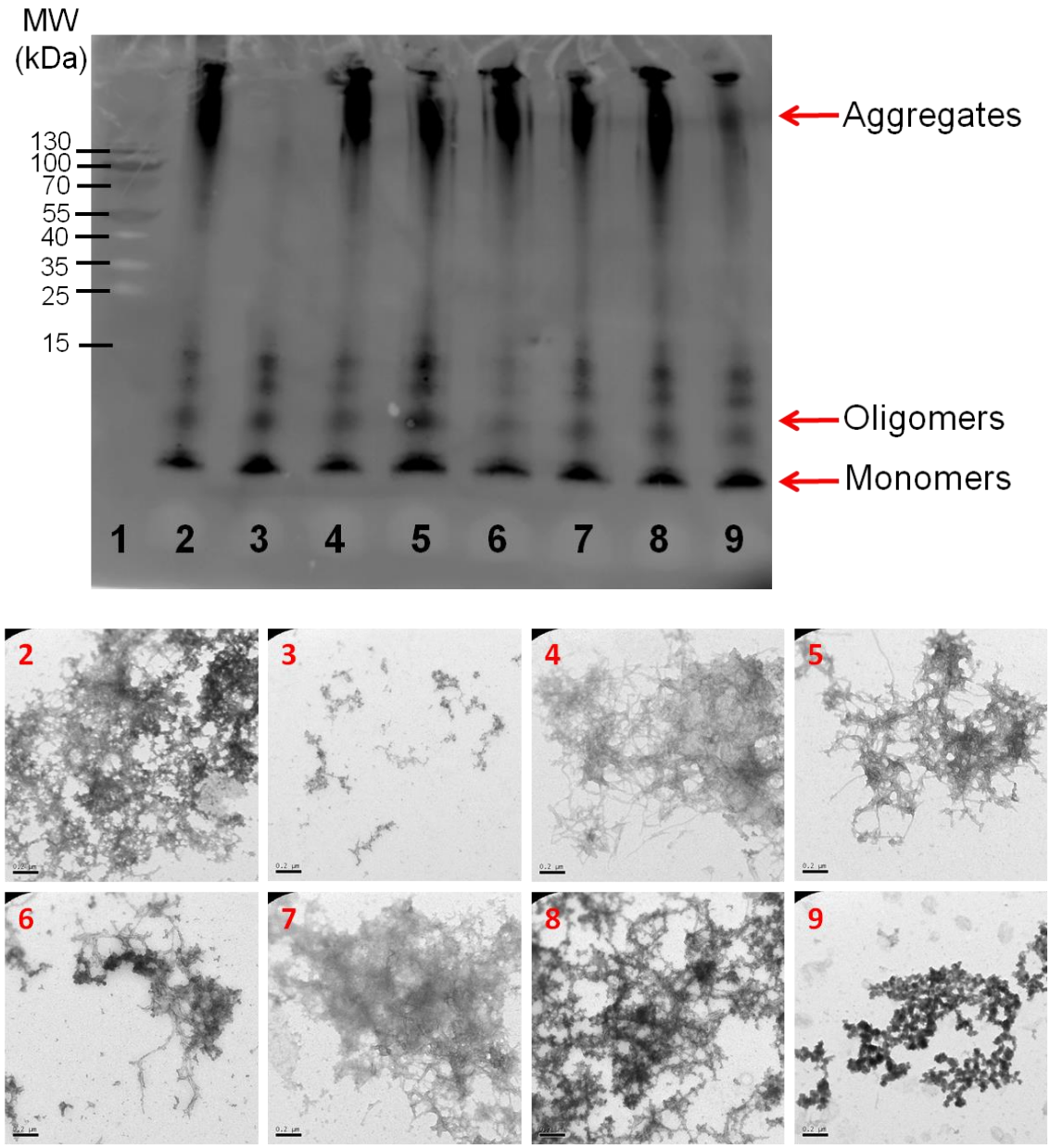

Figure 8. Native Gel/Western blots and TEM images of $A\beta_{1-42}$ aggregation experiments. Top: (**1**) protein reference; (**2**) $A\beta_{1-42}$; (**3**) $A\beta_{1-42}$ + Cu^{II}; (**4**) $A\beta_{1-42}$ + 8-H_2QH (3 equiv); (**5**) $A\beta_{1-42}$ + Cu^{II} + 8-H_2QH (3 equiv); (**6**) $A\beta_{1-42}$ + 8-H_2QS (3 equiv); (**7**) $A\beta_{1-42}$ + Cu^{II} + 8-H_2QH (3 equiv); (**8**) $A\beta_{1-42}$ + PBT2 (3 equiv); (**9**) $A\beta_{1-42}$ + Cu^{II} + PBT2 (3 equiv); bottom: TEM images of the same samples. Conditions: 24 hours with agitation in PBS at 37 °C, [Aβ] = [M] = 25 μM. The scale bar in each TEM image represents 200 nm.

Table 5. Cytotoxic activities of 8-H_2QH and 8-H_2QS compounds against human cell lines.

Cell Line	% Inhibition of cell / viability proliferation		
	8-H_2QS	8-H_2QH	Cisplatin
MDA-MB	8.3 ± 2.1	Inactive	21.2 ±5.1
HL60	Inactive	7.0 ± 3.2	90.3 ± 1.4
Jurkat	Inactive	4. ±2.2	86.6 ± 6.2